Cell Metabolism
Short Article

Loss of the PlagL2 Transcription Factor Affects Lacteal Uptake of Chylomicrons

Frederik Van Dyck,[1,10] Caroline V. Braem,[1,10] Zhao Chen,[6,8] Jeroen Declercq,[1] Rob Deckers,[1] Byeong-Moo Kim,[6,8] Susumu Ito,[7] Michele K. Wu,[8] David E. Cohen,[8] Mieke Dewerchin,[2] Rita Derua,[5] Etienne Waelkens,[5] Laurence Fiette,[9] Anton Roebroek,[3] Frans Schuit,[4] Wim J.M. Van de Ven,[1,*] and Ramesh A. Shivdasani[6,8]

[1]Laboratory of Molecular Oncology, Department of Human Genetics
[2]Center for Transgene Technology and Gene Therapy
[3]Laboratory of Experimental Mouse Genetics, Department of Human Genetics
[4]Gene Expression Unit, Division of Biochemistry
[5]Laboratory for Protein Phosphorylation and Proteomics
University of Leuven, B-3000 Leuven, Belgium
[6]Dana-Farber Cancer Institute
[7]Department of Cell Biology
[8]Department of Medicine, Brigham & Women's Hospital
Harvard Medical School, Boston, MA 02115, USA
[9]Platform of Veterinary Diagnosis, CMU, 1 rue Michel Servet, CH-1211 Geneva 4, Switzerland
[10]These authors contributed equally to this work.
*Correspondence: wim.vandeven@med.kuleuven.be
DOI 10.1016/j.cmet.2007.09.010

SUMMARY

Enterocytes assemble dietary lipids into chylomicron particles that are taken up by intestinal lacteal vessels and peripheral tissues. Although chylomicrons are known to assemble in part within membrane secretory pathways, the modifications required for efficient vascular uptake are unknown. Here we report that the transcription factor pleomorphic adenoma gene-like 2 (*PlagL2*) is essential for this aspect of dietary lipid metabolism. *PlagL2*$^{-/-}$ mice die from postnatal wasting owing to failure of fat absorption. Lipids modified in the absence of PlagL2 exit from enterocytes but fail to enter interstitial lacteal vessels. Dysregulation of enterocyte genes closely linked to intracellular membrane transport identified candidate regulators of critical steps in chylomicron assembly. PlagL2 thus regulates important aspects of dietary lipid absorption, and the *PlagL2*$^{-/-}$ animal model has implications for the amelioration of obesity and the metabolic syndrome.

INTRODUCTION

Pleomorphic adenoma gene-like 2 (*PLAGL2*) is a close homolog of *PLAG1*, a proto-oncogene implicated in various tumors in humans and genetically modified mice (Declercq et al., 2005). Together with the candidate tumor suppressor *PLAGL1*, these genes constitute a subfamily (Kas et al., 1998) encoding transcription factors with a C-terminal transactivation domain and an N-terminal zinc-finger region that recognizes GRGGC(N)$_7$ RGGK motifs in DNA. Although PlagL2 acts as a dominant oncogene in NIH 3T3 cells (Hensen et al., 2002) and has recently been implicated in human acute myeloid leukemia (Landrette et al., 2005), its physiologic functions are unknown. Here we report that *PlagL2* null mice display severe postnatal wasting resulting from failure to absorb dietary lipids.

Most dietary lipids are long-chain triglycerides (TGs) that are digested and absorbed in phases. Gut luminal hydrolysis generates fatty acids and monoglycerides, which form mixed micelles with bile salts and enter mucosal enterocytes, where endoplasmic reticulum enzymes re-esterify them into TGs. Along with cholesterol, cholesteryl esters, phospholipids, and ApoB, these TGs are assembled into chylomicrons (CMs) and released from the enterocyte basolateral surface into the lamina propria. Mutant intestines seem to carry a specific defect in CM metabolism that prevents entry from intestinal lamina propria into lacteal vessels, and they show dysregulated expression of genes closely linked to intracellular lipid metabolism. Little is known about CM modifications that permit their uptake by lacteal vessels; our studies establish a function for PlagL2 in enterocyte CM metabolism that enables such uptake.

RESULTS AND DISCUSSION

Growth Arrest and Lethality of *PlagL2*$^{-/-}$ Mice Due to Starvation

Our targeting strategy deleted *PlagL2* exon 2 (encoding residues 88–496) (Figure 1A), hence disrupting the first zinc finger and removing the following five zinc-finger motifs and the transactivation domain. Although several targeted embryonic stem (ES) cell clones showed

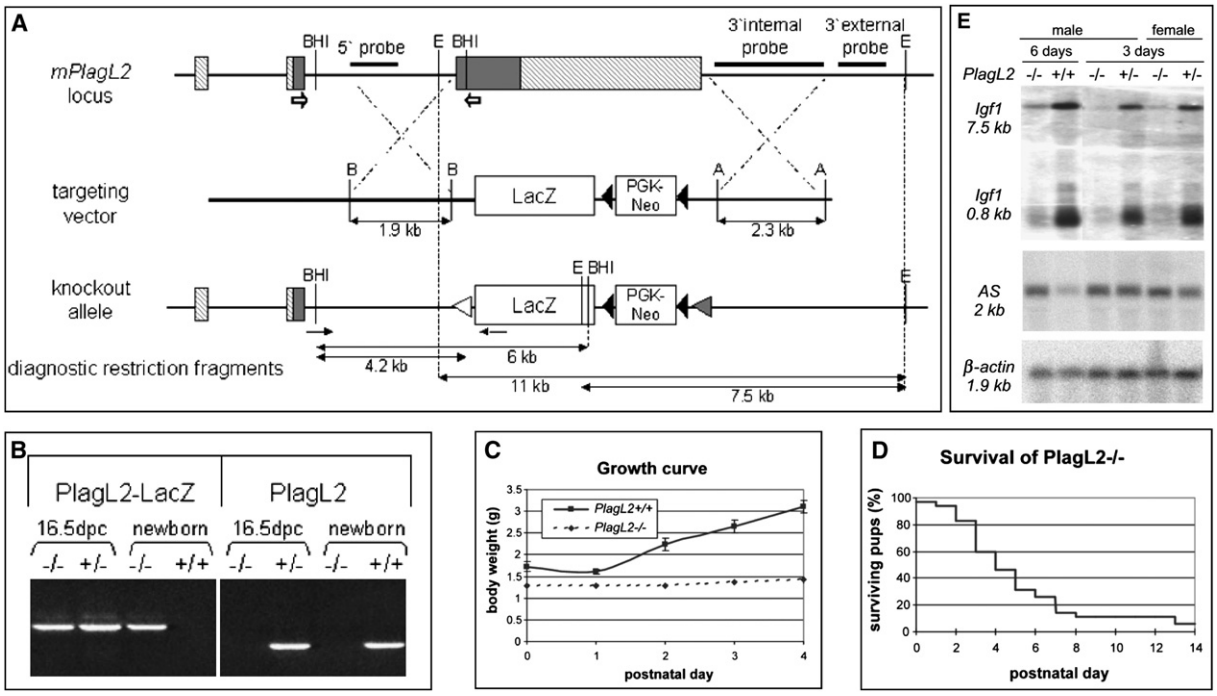

Figure 1. Targeted Disruption of the Mouse *PlagL2* Gene

(A) Representation of the mouse *PlagL2* gene (two coding exons separated by a 3.5 kb intron), targeting vector, and recombined null allele. The targeting construct contains BsrGI (B) and ApaI (A) fragments as 5′ and 3′ homology arms flanking *LacZ* cDNA and a floxed (black triangles) *PGK-Neo* selection cassette. BamHI (BHI) and EcoRI (E) digests yield diagnostic fragments in Southern analysis using one or more of the indicated probes. PCR and RT-PCR with primers corresponding to the short arrows permitted determination of genotypes and expression.

(B) Detection of native *PlagL2* transcripts in *PlagL2*$^{+/-}$ and *PlagL2*$^{+/+}$ samples and of *PlagL2-LacZ* fusion transcripts in *PlagL2*$^{+/-}$ and *PlagL2*$^{-/-}$ samples by RT-PCR analysis.

(C) Growth curves of *PlagL2*$^{-/-}$ pups (dotted line) and littermate controls (solid line) ($p \leq 0.005$; $n \geq 15$ at all stages). Results are expressed as mean values ± SD.

(D) Survival curve of *PlagL2*$^{-/-}$ pups (n = 35).

(E) Northern analysis of the hepatic nutritional markers *Igf1* and *AS* in 3-day-old and 6-day-old *PlagL2*$^{-/-}$ pups.

homologous recombination, one *PlagL2* allele in each line was replaced by a concatemeric form of the targeting construct (see Figure S1A in the Supplemental Data available with this article online). Morula aggregation with targeted ES cells yielded male chimeras and germline transmission of the targeted *PlagL2* allele (*PlagL2*$^{-}$). To allow Cre-mediated excision of concatemer copies (Lallemand et al., 1998), 129/SvJ mutant mice were crossed with Swiss Webster PGK-Cre mice and selected against the *Cre* transgene in the next generation. Intercrossing the resulting heterozygous offspring yielded *PlagL2*$^{-/-}$ pups in Mendelian ratios. We confirmed loss of *PlagL2* and presence of *PlagL2-LacZ* fusion transcripts by RT-PCR (Figure 1B).

PlagL2$^{-/-}$ neonates weighed slightly less than wild-type littermates and subsequently failed to gain weight (Figure 1C). Only 15% of mutant pups survived beyond the first week, and <5% reached weaning age (Figure 1D). mRNA levels of asparagine synthetase (*AS*), a starvation response factor (Jousse et al., 2004), were increased in *PlagL2*$^{-/-}$ livers, whereas *Igf1* expression, which is repressed during starvation (Thissen et al., 1994), was significantly decreased (Figure 1E), indicating that *PlagL2*$^{-/-}$ pups succumb to a wasting syndrome. This early postnatal phenotype contrasts with the predominant expression of *PlagL2* mRNA between 11.5 and 16.5 days postcoitum (dpc) (data not shown). The related *Plag1* gene may compensate for loss of *PlagL2* in developing tissues where both homologs are present. *Plag1* expression levels decline drastically after birth (Hensen et al., 2004), perhaps allowing essential *PlagL2* requirements to be revealed.

PlagL2 Expression in Mouse Small Intestine

Presence of ample milk in the stomachs of *PlagL2*$^{-/-}$ pups suggested that wasting resulted from malabsorption rather than malnutrition, and northern analysis revealed high *PlagL2* mRNA levels in 15.5–18.5 dpc mouse intestines. Expression remained high until weaning and persisted thereafter, albeit at reduced relative levels (Figure 2A). Taking advantage of the *LacZ* reporter inserted in the targeted *PlagL2* allele, we detected β-galactosidase in intestines of 18.5 dpc *PlagL2*$^{+/-}$ embryos (Figure 2B), but not in stomach, liver, pancreas, mesentery, or mesenteric lymph nodes. Histology revealed LacZ staining in intestinal villus epithelial cells, but not in

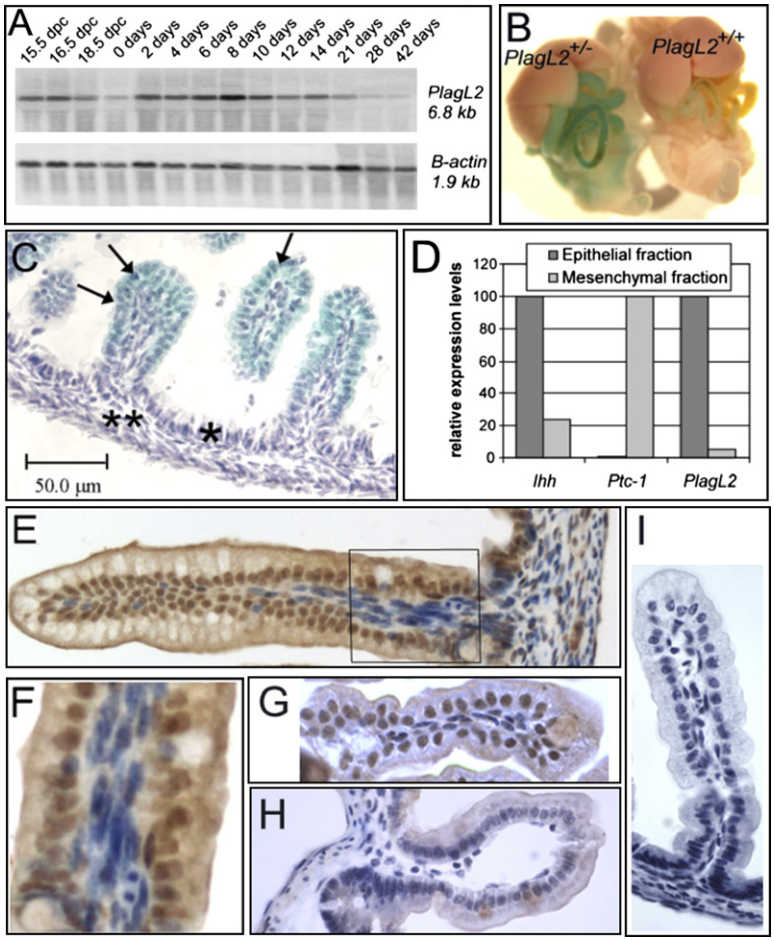

Figure 2. PlagL2 Expression in Developing Mouse Intestine

(A) Northern analysis of *PlagL2* expression at different stages in wild-type mouse small intestine, with β-*actin* as a loading control.

(B) X-gal staining of 18.5 postcoitum (dpc) *PlagL2*$^{+/-}$ and *PlagL2*$^{+/+}$ developing intestines.

(C) Histologic sections of X-gal-stained gut with villus epithelial cells (arrows), intervillus epithelium (*), and mesenchyme (**) indicated.

(D) qRT-PCR confirming *PlagL2* expression in the epithelial fraction. *Ihh* and *Ptc-1* serve as control epithelium- and mesenchyme-specific transcripts. n ≥ 2 for each of the different gene transcripts tested for each fraction. Experiments were performed in duplicate.

(E–G) PlagL2 immunohistochemistry of 3-day-old wild-type small bowel, showing epithelium-specific expression; (F) shows the area boxed in (E).

(H) Immunohistochemistry of *PlagL2*$^{-/-}$ intestine, revealing background cytoplasmic staining and absence of signal in enterocyte nuclei.

(I) Control staining of 3-day-old wild-type small intestine with PlagL2 antiserum omitted.

subepithelial tissue (Figure 2C). We also separated epithelium and mesenchyme of 18.5 dpc intestines and verified enrichment of each fraction by assessing expression of epithelial (Indian hedgehog, *Ihh*) and mesenchymal (Patched 1, *Ptc-1*) transcripts (Madison et al., 2005) by real-time RT-PCR. *PlagL2* mRNA appeared in the epithelial fraction (Figure 2D), as also observed through expression profiling (Li et al., 2007).

Finally, we performed immunohistochemistry on neonatal small bowel sections using rabbit PlagL2 antiserum. We tested antibody reactivity first by immunoblot analysis (Figure S1B). In wild-type gut sections, the antiserum stained nuclei of most villus epithelial cells but few if any subepithelial cells (Figure 2E), as emphasized in high-magnification micrographs (Figures 2F and 2G). Cytoplasmic and smooth-muscle staining also occurred in *PlagL2*$^{-/-}$ intestine, where nuclear staining was absent (Figure 2H), establishing the specificity of the nuclear signal as expected for a transcription factor; omission of the antiserum eliminated all signals (Figure 2I). *PlagL2* mRNA levels are roughly equal in different bowel segments, including the colon (Figure S1C), where protein expression is also epithelial (data not shown). *Plag1* expression in the developing gut is negligible and is not influenced by PlagL2 loss (data not shown).

Defective Lipid Absorption by *PlagL2*$^{-/-}$ Intestine

The lamina propria and submucosa in *PlagL2*$^{-/-}$ small bowel were significantly distended (Figure 3E), and prominent vacuoles in jejunal enterocytes (Figure 3H) were reminiscent of findings in humans and mice with deficiency or absence of intestinal apolipoprotein B (ApoB) (Gregg and Wetterau, 1994; Young et al., 1995). Goblet and enteroendocrine cells were represented in normal proportions (data not shown), and expression of intestinal fatty acid-binding protein (iFABP), an enterocyte marker, was similar to that in control intestines (Figure 4B). These results collectively indicate correct allocation of gut epithelial cell lineages.

Oil red O staining of the mutant gut revealed striking deposition of neutral lipids in the interstitium and accumulation within jejunal enterocytes (Figures 3F, 3G, 3I, and 3J). Thus, whereas *PlagL2* expression is epithelial, histopathological changes in the mutant small bowel concentrate in the lamina propria and, in light of the wasting syndrome, suggest defective lipid absorption. Mutant intestines (n = 5) contained 25.3 ± 1.5 mg TG per gram of wet tissue, compared to 15.0 ± 1.27 mg/g in wild-type littermates (n = 12). This difference is highly significant (p = 0.0003 by two-tailed t test) and probably underestimates TG excess in regions of maximal physiologic lipid absorption

compared to the rest of the intestine. In the proximal gut, which accounts for a small fraction of dietary fat uptake, *PlagL2*$^{-/-}$ mice accumulate modest amounts of interstitial lipid. In the distal jejunum, where over 80% of fat is absorbed, interstitial lipid accumulation in *PlagL2*$^{-/-}$ mice is the highest and lipid excess is evident in enterocytes (Figure 3J), probably because transport systems are overloaded.

Mass spectrometric analysis of independent samples confirmed at least 2- to 3-fold increase in all TG species in the mutant bowel (Table S1), including those derived from saturated, monounsaturated, and polyunsaturated fatty acids. As the latter cannot form in mammalian cells, the presence of 18:2, 20:4, and other such species indicates re-esterification of essential fatty acids and implicates PlagL2 function at a later step in lipid absorption. Notably, cholesterol levels were similar in wild-type (9.7 ± 2.8 mg/g, n = 12, determined enzymatically) and mutant (6.7 ± 1.7 mg/g, n = 5, p = 0.52) intestines; mass spectrometry also disclosed similar phospholipid, cholesteryl ester, and free fatty acid content (data not shown). In contrast to the gut, livers of mutant infant mice showed no increase in TG (5.8 ± 1.0 mg/g, n = 4, compared to 6.0 ± 0.5 mg/g in 12 wild-type littermates; p = 0.85) or cholesterol (5.1 ± 0.1 mg/g, n = 5, compared to 5.3 ± 0.1 mg/g in 12 wild-type littermates; p = 0.33) levels.

Interstitial CMs are normally sparse because they efficiently enter lacteal vessels present in the stalk of each villus. Indeed, transmission electron microscopy (TEM) of *PlagL2*$^{+/+}$ (Figure 3M) and *PlagL2*$^{+/-}$ (data not shown) lamina propria showed CM profiles contained within endothelium-lined channels, whereas *PlagL2*$^{-/-}$ gut interstitium was filled with mature CMs unbounded by endothelium (Figure 3N). *PlagL2*$^{-/-}$ enterocytes exhibited abundant lipid droplets at the apex and ostensibly mature CMs, which have a distinctive ultrastructure, closer to the cell nucleus (Figure 3O). These results reveal intact intracellular CM assembly, and we often observed CMs clustered within vesicles, some of which abutted the basolateral cell membrane (Figures 3O and 3P), suggesting preparation for release. These particles closely resembled CMs in the interstitium (Figure 3P, inset), and lipid collections not only appeared in the lamina propria but also pooled between neighboring enterocytes (Figure 3Q), above the basement membrane. Neither TEM (Figure 3O) nor immunostaining for activated caspase-3 (Figure 4A) revealed mucosal cell apoptosis as a possible source of accumulated CMs. Viable *PlagL2* null enterocytes thus assemble and secrete CMs that fail to exit the gut interstitium.

Nature of the Chylomicron Absorption Defect

In *PlagL2*$^{-/-}$ intestine, capillaries and other lamina propria elements were compressed by excess lipid (Figures 3K and 3L). Although subepithelial CM accumulation could potentially reflect failures intrinsic to lamina propria lymphatic vessels, three independent methods place PlagL2 expression in mucosal cells (Figure 2). Our findings thus suggest a cell-autonomous requirement for PlagL2 in enterocytes, whereby CMs can exit from these cells but lack modifications required for subsequent uptake. Plasma lipid concentrations suggest that CM uptake is impaired not only in the intestine but also in peripheral tissues: 3-day-old mutant mice had elevated circulating TG (101.6 ± 31.1 mg/dl, n = 6, compared to 46.3 ± 4.5 mg/dl in 12 wild-type littermates; p = 0.024) and cholesterol (119.9 ± 36.4 mg/dl, n = 5, compared to 54.9 ± 1.0 mg/dl in 12 wild-type littermates; p = 0.024) levels. The only satisfying explanation for the aggregate mutant phenotype, which includes normal liver lipid levels, is a CM defect that impairs local absorption and subsequent metabolism. Although CM uptake by lacteal vessels is regarded as a passive process (Lammert and Wang, 2005), we propose that PlagL2-dependent steps in CM assembly are needed to enable it. As a result, defective CMs in *PlagL2*$^{-/-}$ mice rarely enter the circulation, and the few that do enter fail to be metabolized within muscle and adipose tissue, leading to cachexia and death.

Known disorders of gut lipid metabolism include lipase and bile salt deficiencies, which cause fat malabsorption (Bijvelds et al., 2005; Lammert and Wang, 2005), and congenital abetalipoproteinemia, a disease in which CMs fail to assemble and long-chain fatty acids are trapped within enterocytes (Hussain et al., 2003). CM synthesis is a complex process that occurs within intracellular secretory pathways; few cellular details are certain, such as the role of ApoB or the small GTPase Sar1b, which is required for intermediate lipids to exit intracellular membrane compartments (Shoulders et al., 2004). Sar1b is defective in CM retention disease and Anderson's disease, rare human disorders characterized by severe fat malabsorption and failure to thrive in infancy (Shoulders et al., 2004). Little is known about the mechanisms responsible for CM uptake into lacteal vessels; our results implicate *PlagL2* in this function.

Molecular Defects in *PlagL2*$^{-/-}$ Intestines

Human *APOB* gene mutations cause betalipoprotein deficiency, and mice lacking intestinal *ApoB* harbor lipid-laden enterocytes (Young et al., 1995); abetalipoproteinemia results from mutations in the microsomal triglyceride transfer protein (*MTTP*) gene (Gregg and Wetterau, 1994). *Mttp* and *ApoB* mRNA levels were comparable in *PlagL2*$^{-/-}$ and *PlagL2*$^{+/+}$ intestine (Figure 4B). ApoB immunohistochemistry in control intestines yielded diffuse cytoplasmic staining in enterocytes, with submucosal signals virtually confined to the contents of lymphatic channels (Figures 4C and 4E). In *PlagL2*$^{-/-}$ enterocytes, ApoB showed the same crypt-villus gradient and perinuclear cytoplasmic enrichment; stronger signals appeared in the interstitium of the lamina propria (Figures 4D and 4F) and between enterocytes (Figure 4G), but not in lymphatic vessels. Thus, significant amounts of ApoB colocalize with CMs detected by other means (Figure 3), and ApoB levels are unlikely to limit enterocyte lipid metabolism.

As there are few other candidate genes to test individually, we used oligonucleotide microarrays to profile small

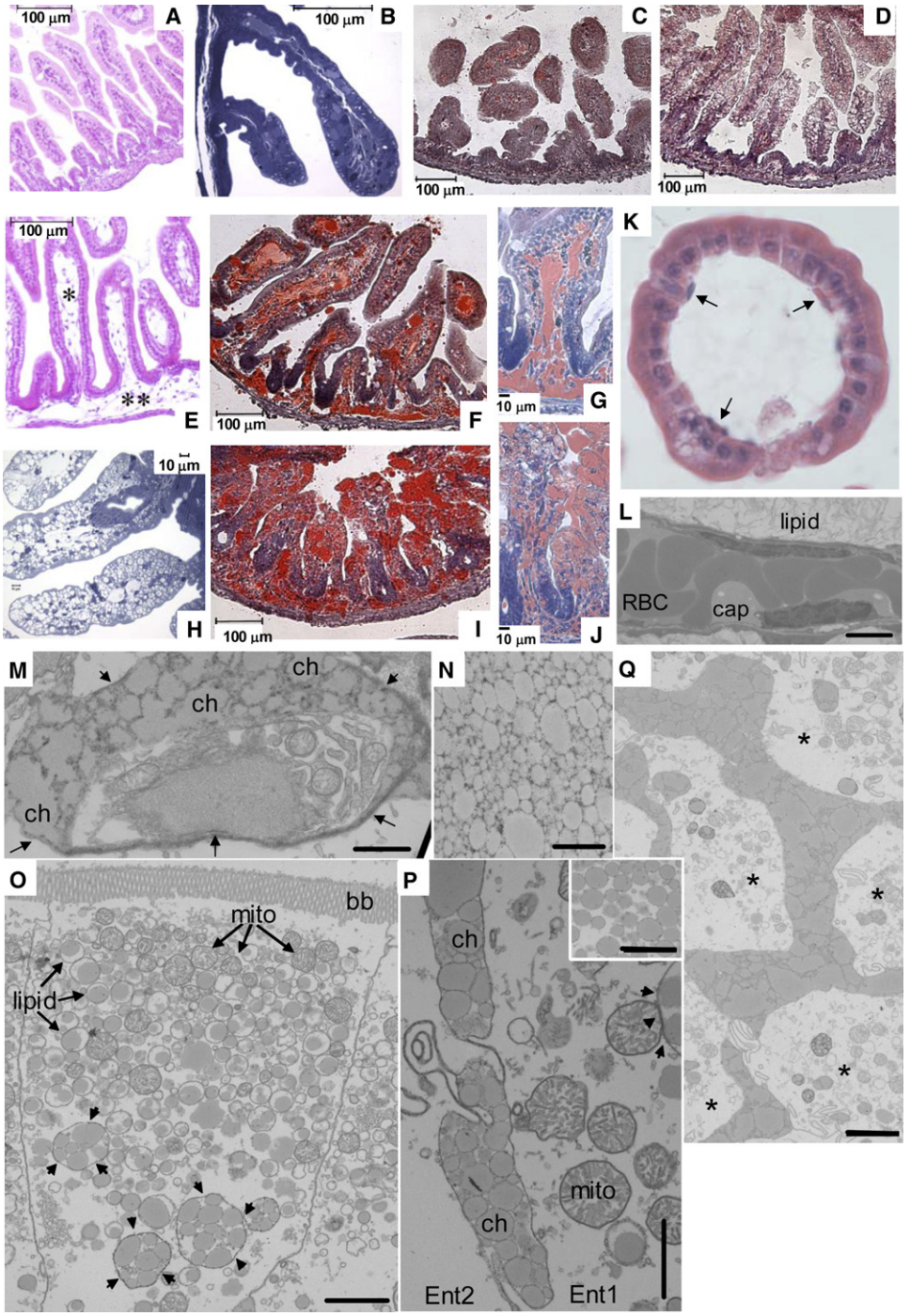

Figure 3. Small Bowel Abnormalities in *PlagL2*$^{-/-}$ Mice

(A, B, E, and H) Hematoxylin and eosin (A and E) and toluidine blue (B and H) stains of postnatal day 8 *PlagL2*$^{+/+}$ (A and B) and *PlagL2*$^{-/-}$ (E and H) jejunum. In the latter, the lamina propria (*) and submucosa (**) are extensively dilated, and villus enterocytes show prominent vesicles.

(C, D, F, G, I, and J) Oil red O staining of frozen sections from 3-day-old *PlagL2*$^{+/+}$ (C and D) and *PlagL2*$^{-/-}$ (F, G, I, and J) small intestine. Extensive interstitial deposition of neutral lipids and fat-laden villus enterocytes are apparent in *PlagL2*$^{-/-}$ jejunum (I and J). Duodenal staining (F and G) is exclusively subepithelial. Control samples (C and D) lack staining.

(K and L) Compression of lamina propria elements (arrows), including capillaries (cap) and erythrocytes (RBC), by excess lipid.

(M–Q) Ultrastructural characterization of the lipid absorption defect in *PlagL2*$^{-/-}$ mice. Scale bars in (L), (O), and (Q) = 2 μm; scale bars in (M), (N), and (P) = 1 μm.

(M and N) Most extracellular chylomicrons (ch) in control (*PlagL2*$^{+/+}$) intestine are surrounded by lymphatic endothelium (arrows) in the lamina propria (M), whereas structures of similar morphology are free in *PlagL2*$^{-/-}$ intestinal interstitium (N).

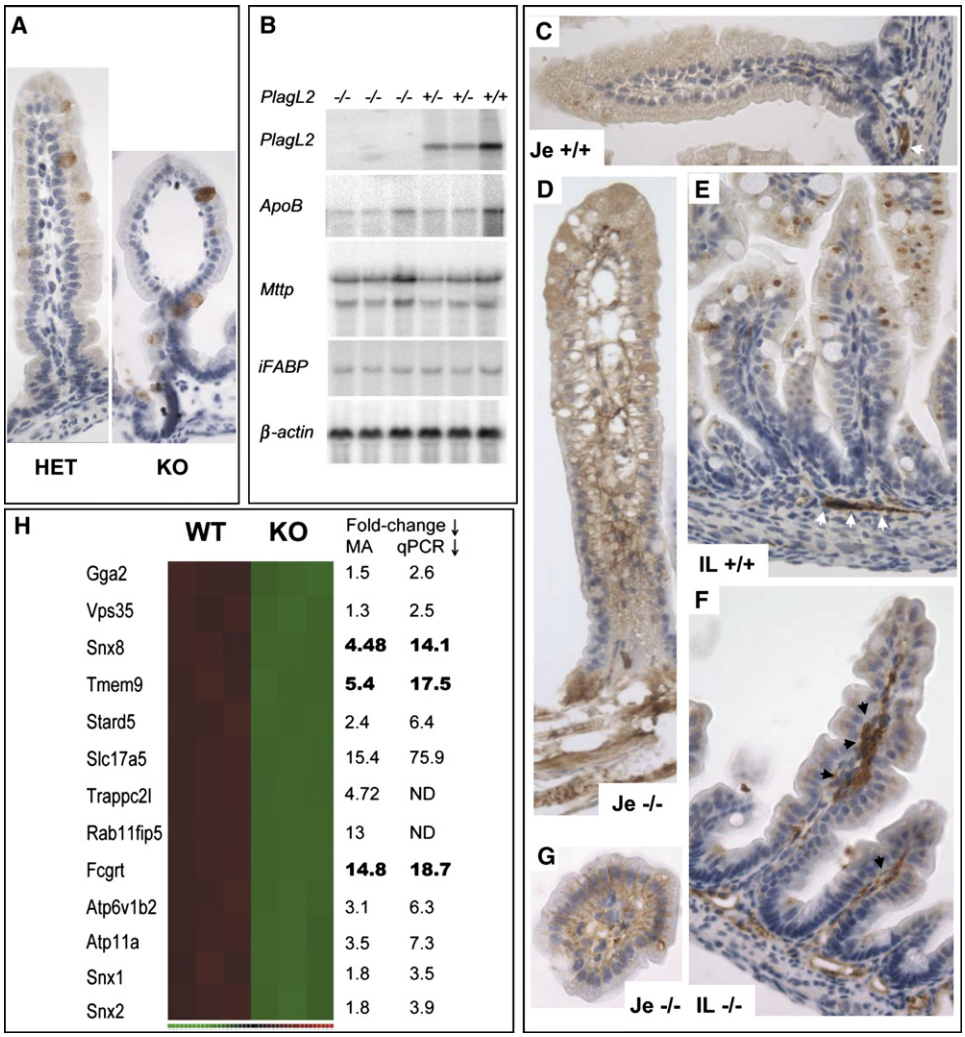

Figure 4. Dysregulated Intestinal Expression of Genes Linked to Lipid Metabolism in the Absence of PlagL2 Function

(A) Immunostaining of *PlagL2*$^{-/-}$ (KO) versus *PlagL2*$^{+/-}$ (HET) intestine for activated caspase-3 failed to reveal excessive enterocyte apoptosis. Goblet cells stained nonspecifically, and a positive control (not shown) confirmed Ab reactivity.

(B) Northern analysis of *PlagL2*, *ApoB*, *Mttp*, *iFABP*, and β-*actin* expression in 2-day-old intestines reveals comparable marker levels in mice of all *PlagL2* genotypes.

(C–G) ApoB immunohistochemistry. *PlagL2*$^{+/+}$ jejunal (Je) and ileal (IL) samples (C and E) show exclusively epithelial staining and some signal within lymphatic channels (white arrows). *PlagL2*$^{-/-}$ intestine shows abundant ApoB in epithelial cells (D), with strong and aberrant signals in gut interstitium (F, black arrows) and pooled between enterocyte bases (G, compare with TEM image in Figure 3Q).

(H) Analysis of a subset of genes whose expression across samples tracked most faithfully with that of *PlagL2* and which, by virtue of affiliation with intracellular secretory pathways, may help explain the particular lipid absorption defect seen in *PlagL2*$^{-/-}$ mice. Levels of dysregulation (fold change) recorded in microarray (MA) and qRT-PCR analyses were concordant in nearly all cases.

bowel gene expression at 18.5 dpc, before severe lipid absorption defects may affect gene expression secondarily. *ApoB* and *ApoAIV* mRNA levels did not differ between wild-type and *PlagL2*$^{-/-}$ mutant samples. Among 301 transcripts that did differ (SD 0.5), hierarchical analysis showed tight clustering within each genotype (Figure S2A), and, in functional grouping by Gene Ontology (GO) criteria, genes implicated in metabolism or in vacuole and transporter activity predominated. Another stringent algorithm, Compare Samples, yielded 164 transcripts with ≥3-fold change between control and mutant samples (Figure S2B). 156 of these transcripts overlapped

(O) Apical lipid-laden vesicles, similar in size to mitochondria (mito), in mutant enterocytes transition into structures that resemble normal chylomicrons, and multiple chylomicrons are contained in secretory vesicles (arrowheads). bb, brush border.

(P) Vesicles packed with chylomicrons (ch) often abut the basolateral cell membrane in *PlagL2*$^{-/-}$ enterocytes (Ent1, Ent2).

(Q) Abundant chylomicron collections pooled between the bases of neighboring enterocytes (*).

with those identified above (Figure S3 and Table S2) and were enriched for two GO functions: metabolism and catalytic activity (39%) and transporter activity (21%). Finally, we isolated transcripts whose expression across all samples tracked with that of the targeted gene; *PlagL2* mRNA showed substantial difference (Table S3), justifying its choice as the index. Analysis of variance ($p < 0.00005$) identified 80 transcripts whose levels across eight samples correlated best with that of *PlagL2*. Of the 68 annotated genes, 40 participate in metabolism or cargo transport (Table S4).

A disproportionate fraction of the genes reduced in *PlagL2*$^{-/-}$ intestine thus serve functions related to intracellular cargo transport, including selected sorting nexins and vacuolar sorting proteins (Figure 4H). The nature of the lipid absorption defect implicates these genes as candidate regulators of intracellular steps in processing dietary fat; some of them likely act to endow CMs with unknown properties that enable interstitial egress and lacteal entry. Quantitative RT-PCR analysis of independent samples verified substantial downregulation of most tested genes, notably *Snx8*, *Slc17a5*, and *Fcgrt* (Figure 4H). Such genes likely fall directly or indirectly under PlagL2 transcriptional control, although some may be misexpressed in physiologic response to lipid accumulation.

Lipoproteins are known to transit through intracellular secretory pathways (Fromme and Schekman, 2005), but understanding of enterocyte CM processing is incomplete. Recent advances implicate the small GTPase Sar1b in CM retention disorders and certain coat and SNARE proteins in transport from the endoplasmic reticulum to the Golgi apparatus (Fromme and Schekman, 2005; Shoulders et al., 2004; Siddiqi et al., 2006). Reduced expression in *PlagL2*$^{-/-}$ gut of sorting nexins and other factors linked to intracellular transport of lipids, membranes, and secretory products is especially relevant in this light.

EXPERIMENTAL PROCEDURES

PlagL2 Mutant Mice

The targeting strategy (Figure 1A) was designed to replace exon 3 (coding exon 2, encoding residues 88–496) of *PlagL2* with β-*gal* cDNA and a floxed *PGK-Neo* cassette. Homologous arms were subcloned from mouse genomic BAC clone 474a11 (Genome Systems), and sequences for β-*gal* and the *PGK-Neo* selection cassette were retrieved from pSDKLacZpA (Gossler et al., 1989) and pPNTLoxP2 (Stalmans et al., 2002), respectively. The complete exogenous sequence was flanked by FRT sites to enable recombinase-mediated cassette exchange. Targeted R1 ES cells were used to generate chimeric mice by morula aggregation. Mice were genotyped by PCR using primers listed in Table S5.

RNA Extraction, Northern Blot Analysis, and RT-PCR

Mouse tissues were snap frozen in liquid nitrogen, and mesenchymal and epithelial fractions from 18.5 dpc small intestines were isolated as previously described (Madison et al., 2005). RNA was extracted in guanidinium isothiocyanate, size fractionated, blotted, and hybridized according to standard protocols. *PlagL2* probe was obtained by digesting pCG-HA-PlagL2 (gift of T. Furukawa, Kansai Medical University, Japan; Furukawa et al., 2001) with BamHI and HindIII. Other probes were generated by PCR amplification using adult mouse liver or gut cDNA and primers listed in Table S5. cDNA was synthesized from 5 μg total RNA using the SuperScript First-Strand Synthesis System (Invitrogen). qPCR reactions were performed with a qPCR MasterMix Plus kit for SYBR green (Eurogentec). Primers for RT-PCR and qPCR are listed in Table S5.

Histology, Immunohistochemistry, and Ultrastructure

Intestines were fixed overnight in 4% paraformaldehyde, and 6 μm paraffin-embedded sections were stained with hematoxylin and eosin or X-gal as previously described (Hensen et al., 2004; Wang et al., 2002). Oil red O staining was done on cryosections. Immunostaining used rabbit PlagL2 antiserum (1:2000) against the C-terminal peptide TSYLPDKLPKVEVDS or ApoB monoclonal Ab 2G11 (1:6000) (Nguyen et al., 2006) and anti-rabbit or anti-mouse ABC kits (Vector Labs). For TEM analysis (Sabesin and Frase, 1977), intestines from neonatal mice were flushed and fixed overnight in 2% OsO_4 diluted 2:1 with 0.1 M phosphate buffer. Samples were postfixed in OsO_4 and embedded in Epon 812. Appropriate thin sections were stained with uranyl acetate and lead citrate and examined in a JEOL 1200 electron microscope at an accelerating voltage of 80 kV.

Lipid Analysis

Tissue and plasma TG and cholesterol concentrations were measured enzymatically (Hyogo et al., 2002). Lipid extraction and reconstitution of *PlagL2*$^{-/-}$ and *PlagL2*$^{+/+}$ small intestinal fractions (3 dpc) for mass spectrometry were carried out as previously described (Milne et al., 2006). Positive-ion ESI MS and tandem MS were performed on a 4000 QTRAP instrument (Applied Biosystems) equipped with a Harvard Apparatus syringe pump operated at 1 μl/min.

Microarray Analysis

Total RNA was extracted from four knockout and four wild-type mouse small intestines at 18.5 dpc using the Macherey-Nagel NucleoSpin kit. cRNA synthesis and labeling, hybridization to Affymetrix MOE430 2.0 expression arrays, and data acquisition were performed using the Affymetrix GeneChip Instrument System. Hybridization data were normalized to an invariant set provided by dChip software (Li and Wong, 2001), and we applied the perfect match (PM)-only model to determine expression values. In hierarchical clustering, 3 of 4 samples from each genotype that clustered best with other replicates were selected for further analysis. Filter Gene and Compare Sample functions in dChip were used, respectively, to extract (1) genes with significant differences between genotypes based on standard deviation across all samples and (2) transcripts with minimum expression value > 80 fluorescence units and $p < 0.05$ for the lower 90% confidence limit on fold change between wild-type and mutant samples.

Supplemental Data

Supplemental Data include three figures and five tables and can be found with this article online at http://www.cellmetabolism.org/cgi/content/full/6/5/406/DC1/.

ACKNOWLEDGMENTS

We thank P. Van Veldhoven, J. Swinnen, and K. Brusselmans for their help with the lipid measurements; B. Vanderschueren, D. Hartmann, and J. Turner for helpful discussions; and R. Milne for ApoB antibody. This work was supported by the "Geconcerteerde Onderzoeksactie" (GOA-08/016), the "Fonds voor Wetenschappelijk Onderzoek Vlaanderen" (FWO, G.0099.02), the "Fortis Bank Verzekeringen-programma voor Kankeronderzoek," the Foundation for Biochemical and Pharmaceutical Research and Education, and the Belgian Federation against Cancer. R.A.S. (R01 DK61139) and D.E.C. (RO1 DK56626 and R01 DK48873) were supported in part by the National Institutes of Health. F.V.D. was supported by the Instituut voor de Aanmoediging van Innovatie door Wetenschap en Technologie Vlaanderen. C.V.B. and J.D. contributed as Aspirants of the FWO.

Received: November 8, 2006
Revised: May 29, 2007
Accepted: September 26, 2007
Published: November 6, 2007

REFERENCES

Bijvelds, M.J., Bronsveld, I., Havinga, R., Sinaasappel, M., de Jonge, H.R., and Verkade, H.J. (2005). Fat absorption in cystic fibrosis mice is impeded by defective lipolysis and post-lipolytic events. Am. J. Physiol. Gastrointest. Liver Physiol. *288*, G646–G653.

Declercq, J., Van Dyck, F., Braem, C.V., Van Valckenborgh, I.C., Voz, M., Wassef, M., Schoonjans, L., Van Damme, B., Fiette, L., and Van de Ven, W.J. (2005). Salivary gland tumors in transgenic mice with targeted PLAG1 proto-oncogene overexpression. Cancer Res. *65*, 4544–4553.

Fromme, J.C., and Schekman, R. (2005). COPII-coated vesicles: flexible enough for large cargo? Curr. Opin. Cell Biol. *17*, 345–352.

Furukawa, T., Adachi, Y., Fujisawa, J., Kambe, T., Yamaguchi-Iwai, Y., Sasaki, R., Kuwahara, J., Ikehara, S., Tokunaga, R., and Taketani, S. (2001). Involvement of PLAGL2 in activation of iron deficient- and hypoxia-induced gene expression in mouse cell lines. Oncogene *20*, 4718–4727.

Gossler, A., Joyner, A.L., Rossant, J., and Skarnes, W.C. (1989). Mouse embryonic stem cells and reporter constructs to detect developmentally regulated genes. Science *244*, 463–465.

Gregg, R.E., and Wetterau, J.R. (1994). The molecular basis of abetalipoproteinemia. Curr. Opin. Lipidol. *5*, 81–86.

Hensen, K., Braem, C., Declercq, J., Van Dyck, F., Dewerchin, M., Fiette, L., Denef, C., and Van de Ven, W.J. (2004). Targeted disruption of the murine Plag1 proto-oncogene causes growth retardation and reduced fertility. Dev. Growth Differ. *46*, 459–470.

Hensen, K., Van Valckenborgh, I.C., Kas, K., Van de Ven, W.J., and Voz, M.L. (2002). The tumorigenic diversity of the three PLAG family members is associated with different DNA binding capacities. Cancer Res. *62*, 1510–1517.

Hussain, M.M., Iqbal, J., Anwar, K., Rava, P., and Dai, K. (2003). Microsomal triglyceride transfer protein: a multifunctional protein. Front. Biosci. *8*, s500–s506.

Hyogo, H., Roy, S., Paigen, B., and Cohen, D.E. (2002). Leptin promotes biliary cholesterol elimination during weight loss in ob/ob mice by regulating the enterohepatic circulation of bile salts. J. Biol. Chem. *277*, 34117–34124.

Jousse, C., Averous, J., Bruhat, A., Carraro, V., Mordier, S., and Fafournoux, P. (2004). Amino acids as regulators of gene expression: molecular mechanisms. Biochem. Biophys. Res. Commun. *313*, 447–452.

Kas, K., Voz, M.L., Hensen, K., Meyen, E., and Van de Ven, W.J. (1998). Transcriptional activation capacity of the novel PLAG family of zinc finger proteins. J. Biol. Chem. *273*, 23026–23032.

Lallemand, Y., Luria, V., Haffner-Krausz, R., and Lonai, P. (1998). Maternally expressed PGK-Cre transgene as a tool for early and uniform activation of the Cre site-specific recombinase. Transgenic Res. *7*, 105–112.

Lammert, F., and Wang, D.Q. (2005). New insights into the genetic regulation of intestinal cholesterol absorption. Gastroenterology *129*, 718–734.

Landrette, S.F., Kuo, Y.H., Hensen, K., Barjesteh van Waalwijk van Doorn-Khosrovani, S., Perrat, P.N., Van de Ven, W.J., Delwel, R., and Castilla, L.H. (2005). Plag1 and Plagl2 are oncogenes that induce acute myeloid leukemia in cooperation with Cbfb-MYH11. Blood *105*, 2900–2907.

Li, C., and Wong, W.H. (2001). Model-based analysis of oligonucleotide arrays: expression index computation and outlier detection. Proc. Natl. Acad. Sci. USA *98*, 31–36.

Li, X., Madison, B.B., Zacharias, W., Kolterud, A., States, D.J., and Gumucio, D.L. (2007). Deconvoluting the intestine: molecular evidence for a major role of the mesenchyme in the modulation of signaling crosstalk. Physiol. Genomics *29*, 290–301.

Madison, B.B., Braunstein, K., Kuizon, E., Portman, K., Qiao, X.T., and Gumucio, D.L. (2005). Epithelial hedgehog signals pattern the intestinal crypt-villus axis. Development *132*, 279–289.

Milne, S., Ivanova, P., Forrester, J., and Brown, H.A. (2006). Lipidomics: an analysis of cellular lipids by ESI-MS. Methods *39*, 92–103.

Nguyen, A.T., Braschi, S., Geoffrion, M., Fong, L.G., Crooke, R.M., Graham, M.J., Young, S.G., and Milne, R. (2006). A mouse monoclonal antibody specific for mouse apoB48 and apoB100 produced by immunizing "apoB39-only" mice with mouse apoB48. Biochim. Biophys. Acta *1761*, 182–185.

Sabesin, S.M., and Frase, S. (1977). Electron microscopic studies of the assembly, intracellular transport, and secretion of chylomicrons by rat intestine. J. Lipid Res. *18*, 496–511.

Shoulders, C.C., Stephens, D.J., and Jones, B. (2004). The intracellular transport of chylomicrons requires the small GTPase, Sar1b. Curr. Opin. Lipidol. *15*, 191–197.

Siddiqi, S.A., Siddiqi, S., Mahan, J., Peggs, K., Gorelick, F.S., and Mansbach, C.M., 2nd. (2006). The identification of a novel endoplasmic reticulum to Golgi SNARE complex used by the prechylomicron transport vesicle. J. Biol. Chem. *281*, 20974–20982.

Stalmans, I., Ng, Y.S., Rohan, R., Fruttiger, M., Bouche, A., Yuce, A., Fujisawa, H., Hermans, B., Shani, M., Jansen, S., et al. (2002). Arteriolar and venular patterning in retinas of mice selectively expressing VEGF isoforms. J. Clin. Invest. *109*, 327–336.

Thissen, J.P., Ketelslegers, J.M., and Underwood, L.E. (1994). Nutritional regulation of the insulin-like growth factors. Endocr. Rev. *15*, 80–101.

Wang, L.C., Nassir, F., Liu, Z.Y., Ling, L., Kuo, F., Crowell, T., Olson, D., Davidson, N.O., and Burkly, L.C. (2002). Disruption of hedgehog signaling reveals a novel role in intestinal morphogenesis and intestinal-specific lipid metabolism in mice. Gastroenterology *122*, 469–482.

Young, S.G., Cham, C.M., Pitas, R.E., Burri, B.J., Connolly, A., Flynn, L., Pappu, A.S., Wong, J.S., Hamilton, R.L., and Farese, R.V., Jr. (1995). A genetic model for absent chylomicron formation: mice producing apolipoprotein B in the liver, but not in the intestine. J. Clin. Invest. *96*, 2932–2946.

Accession Numbers

Microarray data reported herein have been deposited in the Gene Expression Omnibus with the accession number GSE9123.